

# AERODYNAMIC COMPUTATIONS OF ISOLATED FENESTRON® IN HOVER CONDITIONS

E. Mouterde<sup>1</sup>, L. Sudre<sup>1</sup>, A.M. Dequin<sup>1</sup>, A. D'Alascio<sup>2</sup>, P. Haldenwang<sup>3</sup>

<sup>1</sup> EUROCOPTER, Aerodynamic Department,  
Aéroport International Marseille-Provence, 13725 Marignane, France  
e-mail : [edith.mouterde@eurocopter.com](mailto:edith.mouterde@eurocopter.com)

<sup>2</sup> EUROCOPTER, Aerodynamic Department,  
Willy-Messerschmidt-Strasse Tor 1, 85221 Ottobrunn, Germany

<sup>3</sup> MSNM-GP, Laboratoire de Modélisation et Simulation Numérique en Mécanique,  
UMR CNRS 6181 - Universités d'Aix-Marseille. I.M.T. La Jetée Château Gombert,  
38 rue Frédéric Joliot Curie - 13451 Marseille Cedex 20

**Key words: Fenestron®, CFD, Helicopter, Aerodynamics**

## **Abstract:**

The main scope of this study is the numerical simulation of the flow in a Fenestron® for performance prediction purpose. This paper describes the application of overset grid methods for analyzing the flow field of the Fenestron®. The Fenestron® itself, the evolution studied and the experimental program used to define it, are first presented. Then the CFD tools are reviewed, and their adaptation to the ducted tail rotor is explained. The modelling of the Fenestron® using the solver including grids and boundary conditions is explained in detail. The results of numerical studies in hovering flight are compared to experimental data. Flow field visualizations are presented and are used to explain the Fenestron® behaviour. It is shown that the CFD tools used are very valuable to understand the Fenestron® in hover conditions.



## 1. INTRODUCTION

“Fenestron” was initially, in the south of France, the name of a small window. It became a well-known word in the helicopter world when the ducted fan (or fan-in-fin) concept was first developed by Sud Aviation helicopter division in 1968, for the Gazelle helicopter. (Refs. [1], [2] and [3]). Since then the Fenestron® (Fig. 1) is the Eurocopter alternative solution to the conventional tail rotor for light and medium helicopters.



Figure 1 : The Fenestron®

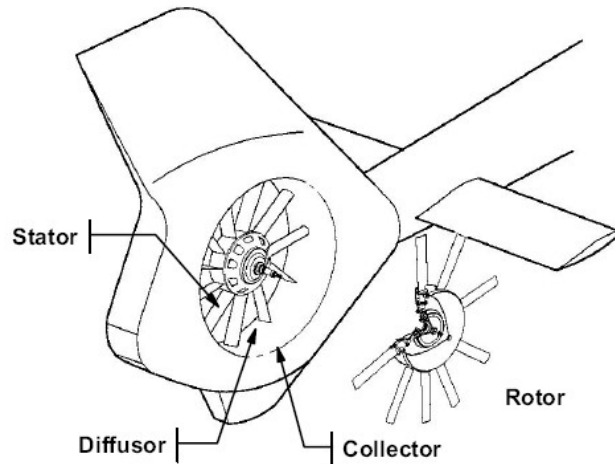


Figure 2 : The Fenestron® components [3]

Like any tail rotor on a classical single main rotor helicopter, the Fenestron® ensures the anti-torque function and the control around the yaw axis. The main advantage, with respect to a conventional tail rotor, is that the fan blades are surrounded by a duct or shroud fairing (Fig. 2), which improves the safety of ground staff and of the helicopter itself when flying close to obstacles (Refs. [4], [5], and [6]). Further it presents improved performance efficiency due to the augmented lift from the duct shroud. It is less prone to the vortex ring state for the lateral wind condition because of much higher induced velocities and thanks to the structure surrounding the fan, which prevents an easy establishment of airflow recirculation. From an acoustic point of view it has a lower noise level in the plane of the fan blade rotation due to the masking effect of the shroud. As noted in Ref. [7], the use of a ducted fan as an anti-torque device provides a remarkable improvement in safety. Since the application of the Fenestron®, no tail rotor blade contact to personnel has been recorded with this antitorque solution.

Within the Eurocopter fleet, the Fenestron® is used on the Dauphin, EC120, EC130 and EC135 helicopters. Recently similar concepts have been tested by other manufacturers like Mitsubishi and Kawasaki in Japan, Kamov in Russia, Boeing-Sikorsky and Bell in the USA.

The main scope of the study reported here is to assess the capability of the current CFD simulations in predicting the hover performance of a Fenestron®. Two different approaches have been considered: the first one with the minimum possible mesh size of a SA365N3 Fenestron®, the second with a comprehensive mesh of the tail of an EC135 helicopter. Experimental results obtained through rotor rig tests are used for validation of the computation results and are first presented. For each approach, the CFD tool is then introduced, the generated mesh described and the flow field solutions presented and compared with the experimental results. The paper ends by drawing the first conclusions and giving some outlook on the future activities planned at Eurocopter.

## **2. THE FENESTRON PERFORMANCE ISSUE**

As for a classical tail rotor the sizing of the Fenestron® is a key issue when designing a new helicopter. Insufficient rotor thrust can lead to helicopter performance limitations or even require a redesign. An over-performing device comes with weight penalties. It is therefore of prime importance to be able to predict the rotor performance with sufficient accuracy.

In the past no numerical tools were available or able to provide enough accurate results on such a complex geometry, therefore analysis was mainly conducted by using empirical methods, based on previous experience on similar design. At Eurocopter the key step forward, as far as the application of CFD to helicopters was concerned, came with the French-German cooperative project CHANCE. The promising validation exercises reported in Refs. [8] to [18] persuaded Eurocopter to validate the capability of CFD tools on the Fenestron® with particular attention to performance prediction.

The available rig tests measurements, gathered in former development campaigns, provided the experimental data basis needed for the validation of the CFD tools and methods. Two numerical approaches were selected: a cheaper and a more expensive one. In the first approach the Fenestron® geometry was simplified as much as possible with the objective of speeding-up the modelling and the computational time, while trying to minimise the loss of accuracy. In the second, the highest level possible of geometrical detail was kept with the disadvantage of having to run very time consuming computations.

In both cases, the goal was not only to correctly predict the performance of the Fenestron® but also to understand the contribution of each element of the Fenestron®. Simplified methods like actuator disk models simulating the ducted rotor effect were thus ignored and only computation with a complete mesh of the blade were considered.

### **2.1. Experiments used for validation**

In the past, the Fenestron® design only relied on experimental data. The full scale hover whirl tower test on the EC135 ducted rotor, conducted in 1993 in Marignane, is presented on Fig. 3. The Fenestron® is oriented so as to blow air upwards and avoid the ground effect. This goal is reached in positive thrust conditions. The measurements are slightly impaired by the ground in negative thrust conditions, which are not a significant problem for Fenestron® sizing.

The tests need to be done by very calm weather, without any wind. The main parameters that are measured during such tests are the thrust and the torque that is transmitted to the Fenestron®. This allows the power curve of the Fenestron® to be derived. Loads survey parameters are also usually observed and recorded but are of little use in the performance analysis.

It can be seen on Fig. 3 that the EC135 Fenestron® encompasses a 10 bladed rotor with uneven spacing as well as a stator that increases the maximum thrust.



Figure 3 : The EC135 Fenestron® on the test rig

Similar tests were also conducted in 1998 on the upgraded Fenestron® that was later installed on the EC155 as well as older versions of the Dauphin family. It incorporates a 10 bladed rotor, unevenly spaced, installed in the existing 1.1m diameter shroud. Because of the use of this existing shroud, this Fenestron® does not incorporate a stator.

The performance measurements on the EC 135 and EC 155 Fenestron® are used here to validate the CFD calculations.

## 2.2. Selected cases

In this study, two different approaches have been considered: the first one with the minimum possible mesh size of a SA365N3 Fenestron®, and the second with a complete mesh of the tail of an EC135 helicopter. Both calculations aim to hover performance calculations in a first time. The EC135 mesh can however be used for any kind of calculation, whereas the second one takes benefit of the rotor symmetry and is therefore limited to purely axial flight computations.

### 2.2.1.SA365N3 Fenestron® with a simple method

The asymmetrical distribution of the 10 blades in the Dauphin's Fenestron® has been introduced to spread the acoustic energy in a broader frequency band, thus reducing its human perception. It has been seen during rig tests that it has little influence on the Fenestron® performance. As the current numerical analysis focuses on this aspect, the blade distribution can be considered in the analysis as equal-spaced. With this assumption the geometrical model can be simplified by representing only a section of one-tenth of the Fenestron®, comprising one blade in an axisymmetric duct without stator and applying periodic boundary conditions. This mesh configuration was selected to decrease as much as possible the computation response time. This configuration is however only possible for hovering and axial flight.

### 2.2.2.EC135 Fenestron® with a comprehensive description

The complete tail of the EC135 comprising the Fenestron® with all its components, *i.e.* the 10 bladed rotor, the rotor hub, the duct with the vertical fin, the stator and the drive shaft fairing have been modelled (Fig. 14). The main advantage is that the model can be used for hover as well as for forward flight conditions, accounts for the aerodynamic interference between the various components and can be used, coupled with a noise prediction tool, to predict the noise emission. The main disadvantage is that a high number of cells is required (circa 22 millions), thus the memory occupation and the CPU time are also high.

### 3. RESULTS

#### 3.1. Simple model of the SA365N3 Fenestron®

##### 3.1.1. Aerodynamic solver general description

The *elsA* (*ensemble logiciel pour la simulation en Aérodynamique*) solver [13], developed by ONERA, is used in the study based on the simple model. This multi-application object oriented aerodynamic code is based on a cell-centred finite volume formulation for multiblock structured meshes. It allows simulating a wide range of aerospace configurations such as aircraft, space launchers, turbo machinery, or helicopters. Several time discretization schemes are available to perform the unsteady computations. Explicit or implicit schemes, or the Gear method, are available.

In the present paper, the implicit scheme is used to perform all the steady computations. The *elsA* solver contains many turbulence models. The turbulent computations presented in this paper use the two equations Wilcox  $k-\omega$  model with the Zheng limiter and correction of Kok.

The Chimera method, used in this study, simplifies the process of structured mesh generation for complex geometry and relative moving bodies. It allows the computation of meshes made of overset grids. The Chimera technique [14] consists in an overlapping boundary condition and a masking condition for areas corresponding to a solid body. For both types of boundaries, the transfer of conservative and turbulent variables is carried out by interpolation.

##### 3.1.2. Grid topology and computation details

In order to reduce the calculation time mainly by simplifying the volume mesh, a sector consisting of one-tenth of a Fenestron® was retained in this study (Fig. 6).

The numerical studies are based on the simplified Fenestron® geometry shown in Fig. 15. Note that all the horizontal stabilizers have been removed, leaving behind an axisymmetric duct wall. Viscous surface boundary conditions are used on the solid surfaces of the blade and shroud grids. The effect of the remaining part of the Fenestron® is computed by taking into account periodic boundary conditions.

##### *Blade Mesh*

This blade grid allows to fill properly the gap between the blade tip and the duct inner surface. As the tip-gap is very small (a few millimetres), a specific care was needed to mesh this region. The blade root and the attachment between the blade and the hub are not modelled. Indeed the forces applied in this zone are considered as very low and thus negligible versus the global thrust of the Fenestron®. The mesh consists in a C topology around the blade to facilitate the calculation of the boundary layer and an O topology inside the profile section in the extension of the blade. The mesh is generated in order to have a round blade tip, which adapts perfectly to the shape of the duct (Fig. 4). The total number of cells in the blade mesh is 1.26 million.

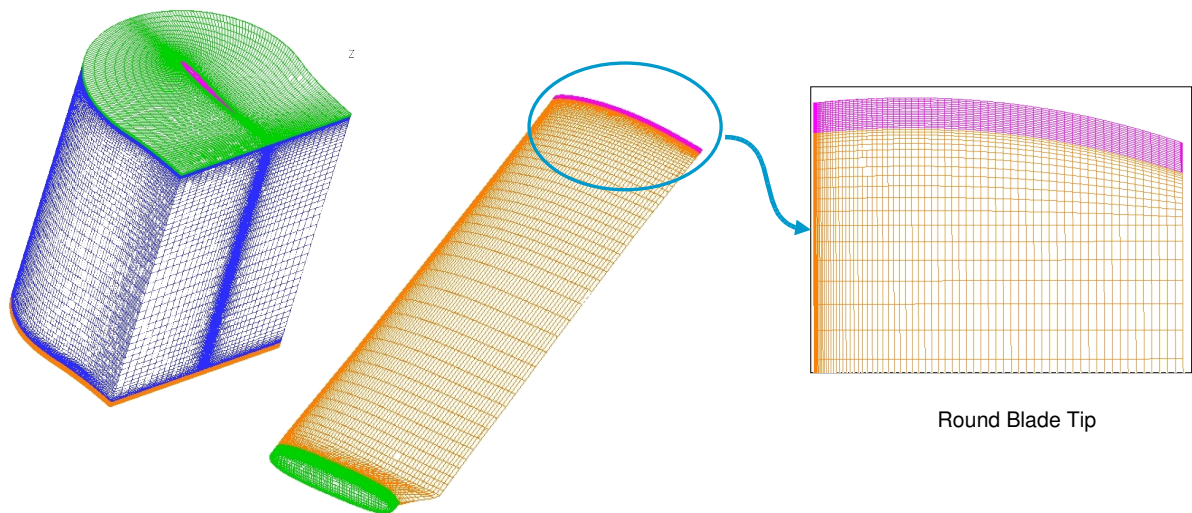


Figure 4 : Blade mesh with round blade tip.

### *Duct Mesh*

A sector of one-tenth of the duct (Fig. 5) is used for the mesh. As for the blade tip mesh the shroud mesh must be refined significantly because of the strong gradients that exist in the vicinity of the blade tip. The duct mesh has 2.46 millions cells.

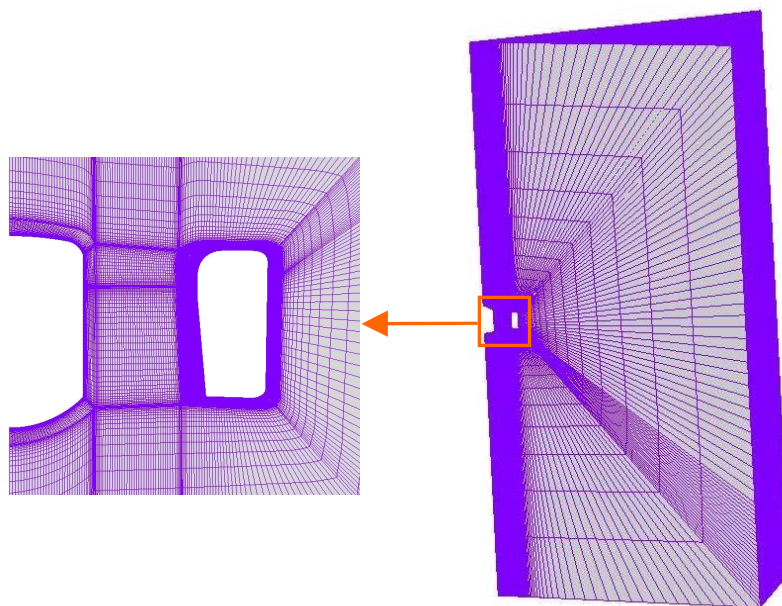


Figure 5 : Duct mesh of one-tenth Fenestron®.

### *Chimera Method*

For the aerodynamic analysis of the Fenestron® a “Chimera” method was applied. From a manufacturer point of view, the main advantages of the “Chimera” method are:

- to ease the mesh generation around complex geometries;
- to allow a reuse of the mesh system for slightly different geometrical configurations.

In this specific case, the chimera method allowed rotating the blade mesh around the feathering-axis, thus changing the pitch angle without any modification of the blade and duct meshes (Fig. 6). A pitch variation is therefore largely facilitated and allows producing many results without increasing the mesh generation time.

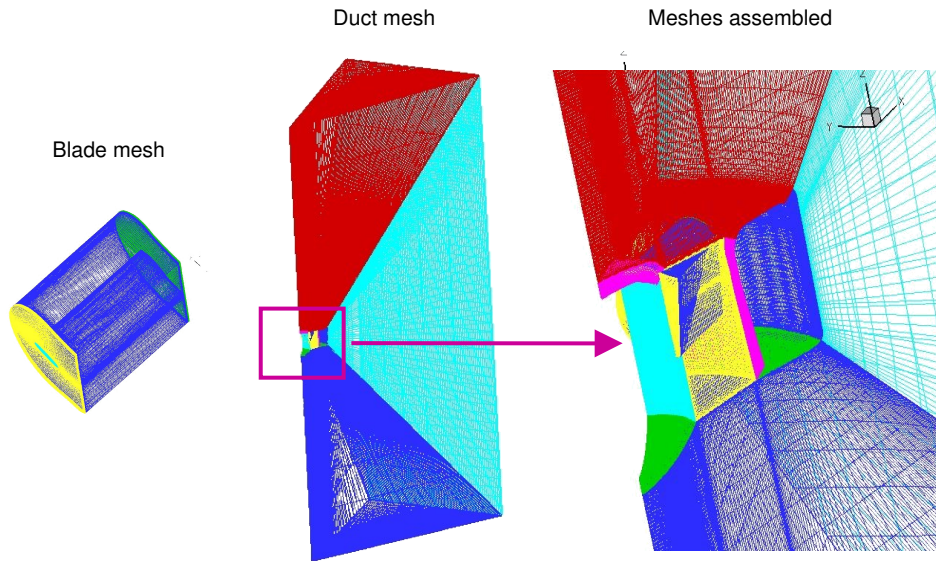


Figure 6 : Integration of the Blade mesh inside the Duct mesh with the Chimera method.

### 3.1.3. Numerical results

For the steady aerodynamic simulations, 3000 iterations were performed. Fig. 7 shows the thrust convergence during calculation for the hover flight in the whole range of the computed pitch angles.

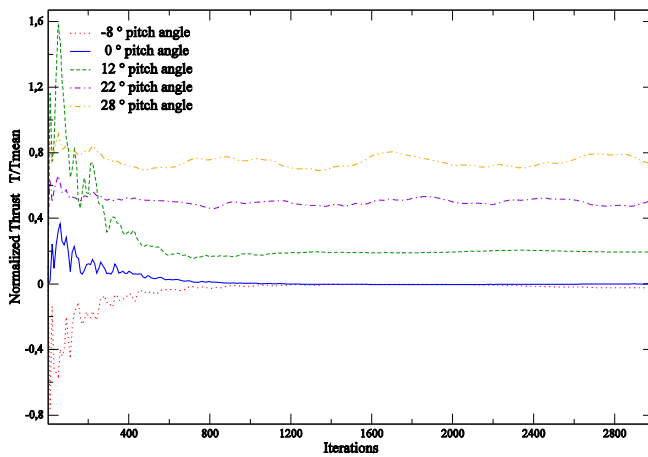


Figure 7 : Thrust convergence

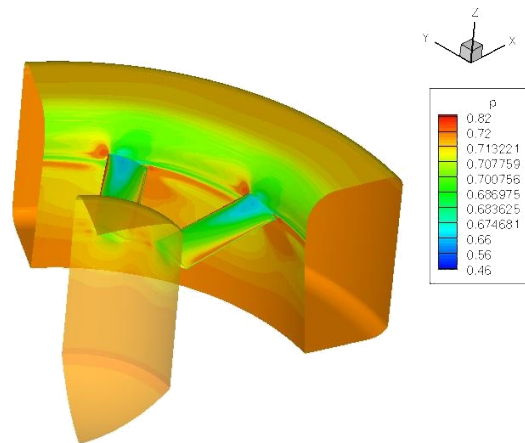


Figure 8 : Pressure distribution on two-tenths of Fenestron®.

Fig. 8 presents the pressure distribution on the blade and on the duct in hover flight. The effect of the blade passage can be seen on the duct. The continuity of the pressure distribution between the two-tenths of Fenestron® shows that the periodicity has well been well integrated. Furthermore the diminution of the pressure in the part of the Fenestron® vein located upstream and the increase in the part of the vein located downstream can be noticed.

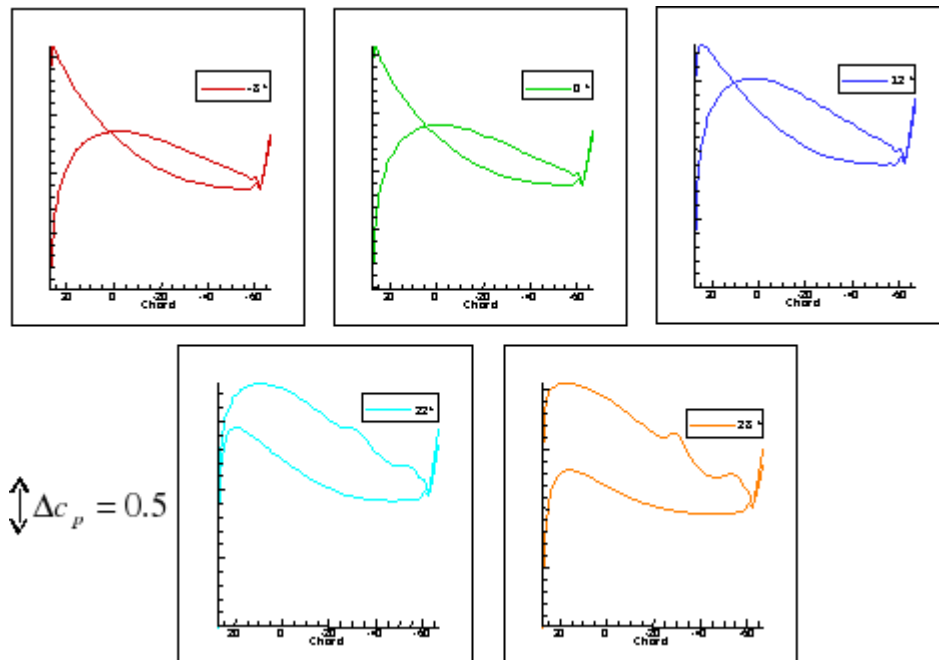


Figure 9 :  $c_p$  versus the chord at the  $0.7R$  radius. (Leading edge in the positive axis direction)

Fig. 9 presents the distribution of the pressure coefficient  $C_p$  along the blade chord for a radius at  $0.7R$ . At this radial station the beginning of oscillations on the  $C_p$  curve on the blade suction side for a pitch angle of  $22^\circ$  is predicted. This is due to a beginning of stall of this blade section. These oscillations are due to the presence of a vortex from the trailing edge to the middle of the cord.

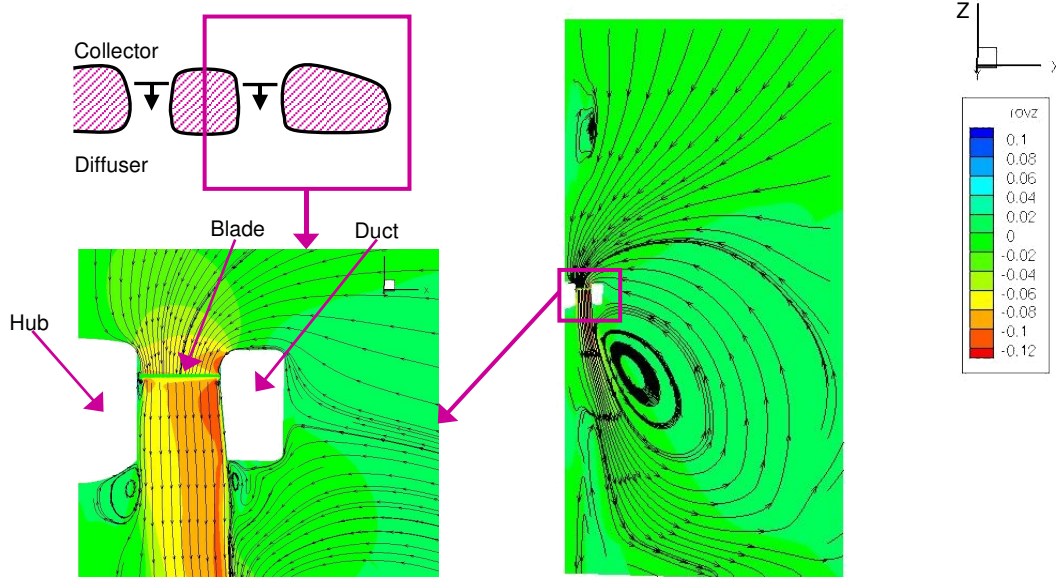


Figure 10 : Visualization of the flow field on an axial plane through the Fenestron® blade for a  $14^\circ$  pitch angle.

Flow field visualizations are presented and are used to explain the ducted fan behaviour. By extracting a section, the streamlines crossing the Fenestron® can be observed. The Fig. 10 clearly reveals the recirculation flow pattern around the duct.

Fig. 11 presents the comparison of the thrust for a range of blade pitch angle between data obtained at the whirl tower and the CFD results. The total thrust on the fan-in-fin is made of two contributions : rotor thrust and shroud thrust which accounts each for about one half of the total thrust. The

computed Fenestron® thrust can be distributed between fan, duct and hub, much more easily than with the experimental approach. The quasi null thrust of the hub and the total thrust which is divided into two equal parts provided by the duct and the rotor can be distinguish. The numerical results confirm that the duct produces approximately the same thrust as the fan.

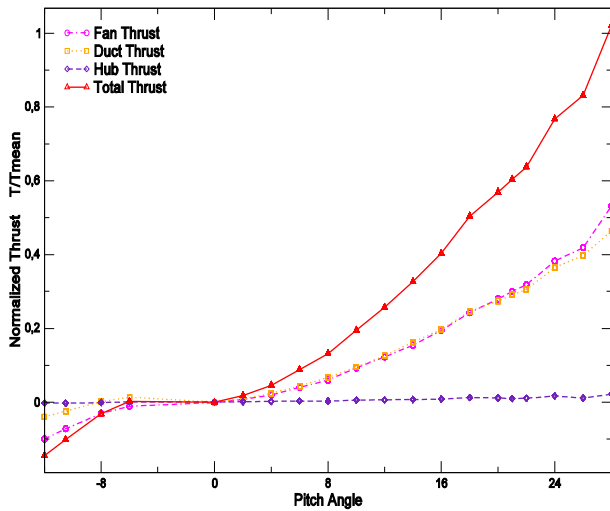


Figure 11 : Distribution of the total Fenestron® thrust between fan, duct and hub.

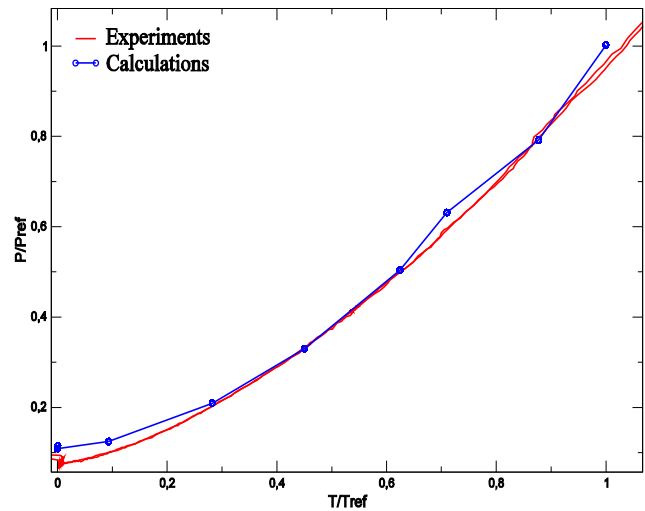


Figure 12 : Comparison between *elsA* results and experimental data

Fig. 12 shows the comparison between the experimental results obtained for Fenestron® of Dauphin in a hover flight and *elsA* results. The computations are in a good agreement with experimental values.

## 3.2. Complete Model

### 3.2.1. Aerodynamic solver general description

The FLOWer flow solver, Refs. [15] and [16], is the Navier-Stokes code developed by DLR, which is being enhanced for rotorcraft applications within the frame of the Franco-German CHANCE, Refs. [17] and [18], research project. It solves the compressible, three-dimensional unsteady Reynolds-averaged Navier-Stokes equations on block structured meshes around bodies in arbitrary motion. FLOWer implements two different spatial discretization schemes, based on finite volume formulation, where the flow variables are located either at the vertices or at the cell centres.

The baseline method employs a central space discretization with artificial viscosity and an explicit five stage Runge-Kutta time integration scheme. Local time-stepping, implicit residual smoothing and multigrid are used to accelerate convergence. Turbulence is modelled by algebraic or by advanced transport equation models, *e.g.* the 2-equation  $k-\omega$  model or the 7-equation Reynolds Stress. Low velocity preconditioning, deforming meshes and the Chimera technique are also available.

### 3.2.2. Grid topology and computation details

Parallel to the aerodynamic study on a 10<sup>th</sup> of a Fenestron®, unsteady CFD computations are performed by using the FLOWer flow solver [15] around the complete geometry of the EC135

Fenestron® with its tail (Fig. 13). These complex, CPU time consuming simulations will be used as a reference for comparisons with more simplified approaches, which can be applied in optimization loops, with the objective of improving the performance of the Fenestron® both in hover and in forward flight.

Also in this numerical analysis the chimera technique was used to ease the mesh generation around such a complex geometry and, at the same time, to allow for a pitch variation without having to modify or adjust any of the meshes.

The overlapping mesh system around the complete tail of the EC135 including the Fenestron®, depicted in Fig. 13, set-up in collaboration with DLR, consists of 10 identical blade fitted meshes, embedded in a circular rotor hub mesh. This subsystem, together with the adjacent stator mesh, is embedded into the tail mesh. An automatically generated background Cartesian multiblock mesh contains the whole system. The complete Chimera system is composed of 21.2 Million nodes distributed over 675 Blocks. Three level of multigrid were assured. FLOWer was run with the following numerical setting: Jameson central space scheme with artificial dissipation, dual-time stepping method for the time discretization and the Wilcox  $k-\omega$  turbulence model. The flow was considered fully turbulent, thus no-laminar transition was accounted for. All unsteady computations were carried out by DLR on a multiprocessor NEC-SX8 supercomputer.

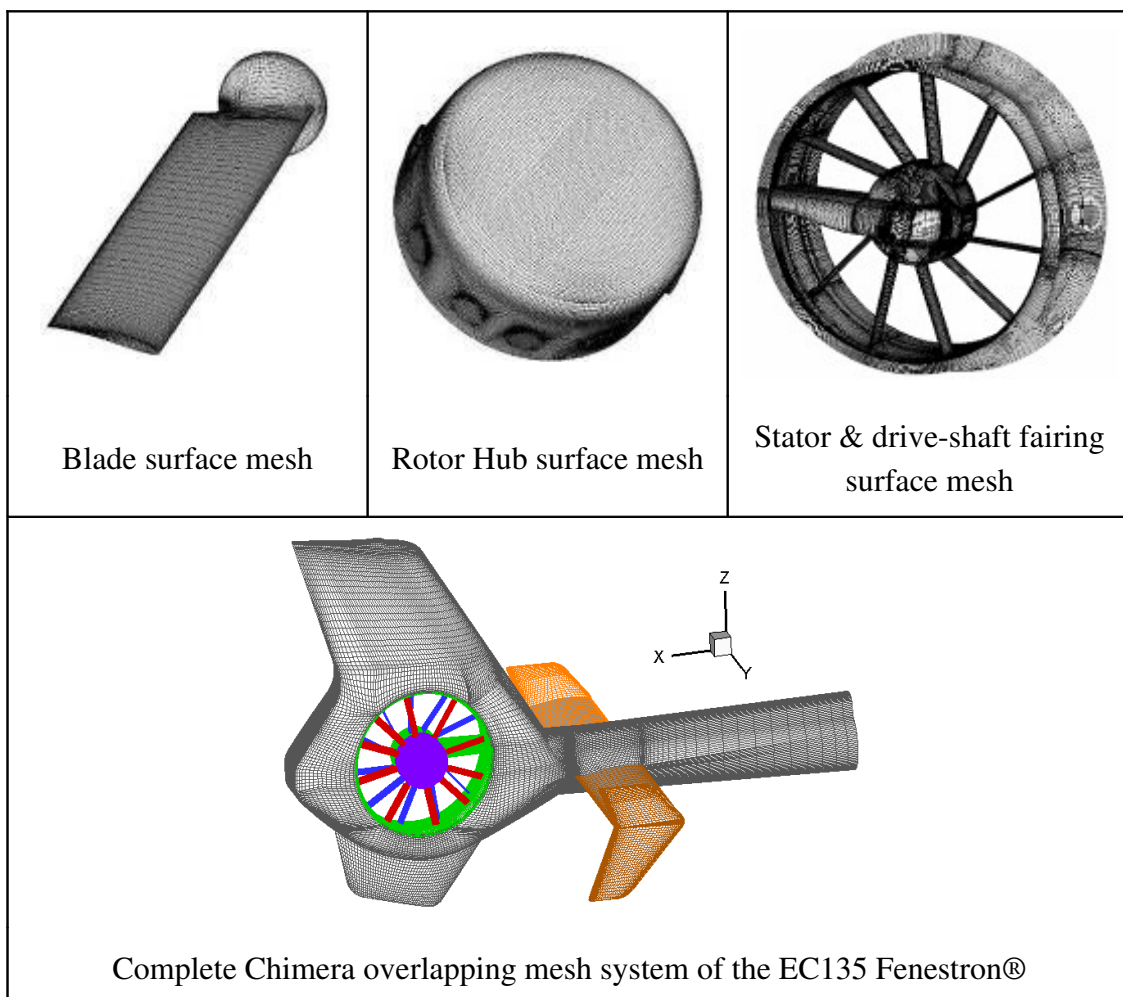


Figure 13 : Chimera system of the EC135 tail with its Fenestron®, comprising rotor, stator and drive-shaft fairing

### 3.2.3.Numerical results

Fig. 14 shows the comparison between FLOWer results, in hovering flight on the above described grid system, and test bench data derived from the EC135 and EC130 Fenestron® measurements carried out by Eurocopter, following the procedure described in Section 2.1. Three rotor revolutions were needed to reach a quasi-periodic solution. The values used to draw the polars are mean values obtained by averaging over the last rotor revolution. The agreement is fairly good in the whole investigated blade pitch-range. Apart from validation purposes of the FLOWer tool and its Chimera interpolation module, this analysis had the main objective of investigating the thrust distribution over the various components of the EC135 Fenestron®, such as the rotor, the duct, the stator and the drive shaft fairing. The results will allow Eurocopter to highlight areas for improvements of the Fenestron® efficiency.

Fig. 15 shows a screen shot of the pressure distribution at the highest computed thrust value of  $T=T'_{Ref}$  on the Fenestron® surface. Here it can be noticed that, apart from the low pressure values occurring on the suction side of the blades, a relatively large region of low pressure is also found on the duct inflow-side, especially on the rounded Lip.

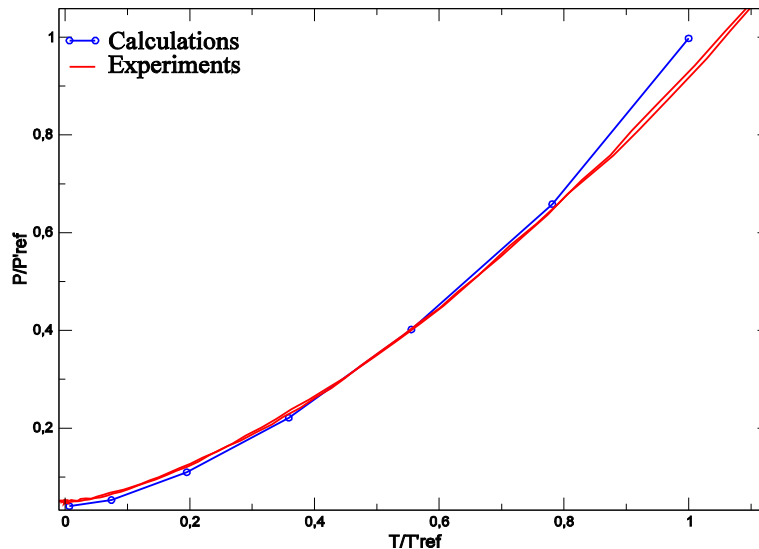


Figure 14 : EC135 Fenestron® Polar curve: Comparison between FLOWer results and the test bench measurements.

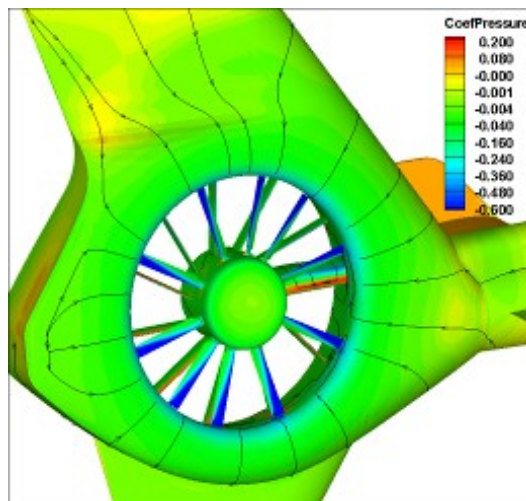


Figure 15. Pressure coefficient distribution on a complete EC135 tail configuration (hover,  $T=T'_{Ref}$ )

## 4. CONCLUSIONS

A numerical approach aiming at the evaluation of the performance of the Fenestron® has been presented. The flow solvers *elsA* and FLOWer have been validated on two different Fenestron® geometries and CFD modelling approaches in hovering flight conditions by comparing the respective numerical prediction results with test bench data. In both cases the agreement was good. The use of the Chimera interpolation technique on overlapping meshes made possible the simplification of the mesh generation approach and the blade pitch variation – necessary to automatically generate a polar – without having to modify or adjust any mesh of the Chimera system.

These encouraging results show that CFD is indeed a valuable tool to study first and improve subsequently the Fenestron® efficiency. The simple method, with much shorter time response, will be used in the future to investigate the influence of most of the relevant design parameters. Furthermore future efforts will be directed toward the axial flight.

The next challenge will however be the more complex level flight case. The simple method is no longer suited for these calculations and only the complete model shown in Chapter 3.2 can be used, with fully unsteady computations, and consequently large CPU time consumption. Improvement of CFD flow solvers in the direction of decreasing the turn around time will be a key factor to bring this type of simulation in the industrial design loop.

## ACKNOWLEDGEMENTS

This research presented in this paper was partially funded by the French DPAC (Direction des Programmes de l'Aviation Civile) and by the German BMWi (Bundesministerium für Wirtschaft and Technologie).

## REFERENCES

- [1] R. Mouille, “The ‘Fenestron’, Shrouded Tail Rotor of the SA. 341 Gazelle”, *Journal of the AHS*, October 1970.
- [2] R. Mouille, “The ‘Fenestron’ – a Shrouded Tail Rotor Concept for Helicopters”, 42<sup>nd</sup> AHS Forum, Washington, DC, June 1986.
- [3] M. Vialle, G. Arnaud, “A new Generation of Fenestron Fan-in-Fin Tail Rotor on EC135”, 19<sup>th</sup> European Rotorcraft Forum, Cernobbio, Italy, September 1993.
- [4] R. Mouille, “Ten years of Aerospatiale experience with the Fenestron and conventional Tail Rotor”, 35<sup>th</sup> AHS Aerospace Sciences Meeting and Exhibit, Washington, DC, May 1979.
- [5] A. Vuillet, “Operational Advantages and Power Efficiency of the Fenestron as compared to a Conventional Tail Rotor”, *Vertiflite*, Vol.35, No. 5, pp. 24-29, July/August 1989.
- [6] R. Prouty, “The Pros And Cons Of The Fan-In-Fin”, *Rotor and Wing*, pp. 54-55, November 1992.

- [7] M.G. Clemmons, “Antitorque Safety and the RAH-66 FANTAIL™”, 48<sup>th</sup> AHS Forum, Washington, DC, June 1992.
- [8] R.G. Rajagopalan, C.N. Keys, “Detailed Aerodynamic Design of the RAH-66 FANTAIL™ Using CFD”, 49<sup>th</sup> AHS Forum, St. Louis, Missouri, May 1993.
- [9] E. Alpman, L.N. Long, B.D. Kothmann, “Toward a Better Understanding of Ducted Rotor Antitorque and Directional Control in Forward Flight”, 59<sup>th</sup> AHS Forum, Phoenix, AZ, May 2003.
- [10] T. Nygaard, A. Dimanling, E. Meadowcroft, “Application of a Momentum Source Model to the RAH-66 Comanche FANTAIL™”, AHS 4<sup>th</sup> Decennial Specialist’s Conference on Aeromechanics, San Francisco, CA, January 2004.
- [11] G. Ruzicka, R. Strawn, E. Meadowcroft, “Discrete Blade CFD Analysis of Ducted Tail Fan Flow”, 42<sup>nd</sup> AIAA Aerospace Sciences Meeting and Exhibit, Reno, Nevada, January 2004.
- [12] P. Gardarein, S. Canard, J. Prieur, “Unsteady Aerodynamic and Aeroacoustic Simulations of a Fenestron Tail Rotor”, 62<sup>th</sup> AHS Forum, Phoenix, Arizona, May 2006.
- [13] M. Gazaix, A. Jollès, M. Lazareff, “The elsA Object-Oriented Computational Tool for Industrial Application”, 23<sup>rd</sup> Congress of ICAS, Toronto, Canada, September 2002.
- [14] C. Benoit, “Synthesis of ONERA Chimera Method Developed in the Frame of CHANCE Program,” 31<sup>st</sup> European Rotorcraft Forum, Florence, Italy, September 2005.
- [15] N. Kroll, B. Eisfeld, H.M. Bleecke, “The Navier-Stokes Code FLOWer”, *Notes on Numerical Fluid Mechanics*, Vol. 71, pp. 58-71. Vieweg, Braunschweig, 1999.
- [16] N. Kroll, C.-C. Rossow, K. Becker, F. Thiele, “The MEGAFLOW Project”, *Aerospace Sciences Technology*, Vol. 4, pp. 223-237, 2000.
- [17] M. Costes, K. Pahlke, A. D’Alascio, C. Castellin, A. Altmikus, “Overview of results obtained during the 6-year French-German CHANCE project”, 61<sup>st</sup> AHS Forum, Grapevine, TX, June 2005.
- [18] K. Pahlke, M. Costes, A. D’Alascio, C. Castellin, A. Altmikus, “The 6-year French-German CHANCE project”, 31<sup>st</sup> European Rotorcraft Forum, Florence, Italy, September 2005.